Journal of Alloys and Compounds 590 (2014) 406–410

Contents lists available at ScienceDirect

Journal of Alloys and Compounds

journal homepage: www.elsevier.com/locate/jalcom

Facile synthesis of ceria nanoparticles by precipitation route for UV blockers

K. Anupriya, E. Vivek, B. Subramanian *

ECMS Division, Central Electrochemical Research Institute, Karaikudi 630 006, India

ARTICLE INFO

Article history:
Received 30 October 2013
Received in revised form 13 December 2013
Accepted 16 December 2013
Available online 21 December 2013

Keywords:
Cerium oxide nanoparticles
Mixed solvent
Precipitation route
UV absorption

ABSTRACT

Homogeneous ceria (CeO_2) nano particles of approximately 4 nm have been successfully synthesized via a simple precipitation route by employing the mixed solvent method. X-ray diffraction analysis revealed the precipitate particles to be of highly crystalline nature with face centered cubic structure along (111) (200) (220) (311) (400) (331) (422) (511) planes. Cerium oxide nanoparticles exhibits enhanced specific surface area of about 139.116 m^2/g. The mono-dispersed spherical shape morphology of approximately 4 nm particles was confirmed using TEM analysis and its chemical composition by SEM–EDS analysis. Surface morphology reveals the smooth surface with an average roughness of 14.9 nm with the help of AFM. Raman studies show a characteristic peak at 464 cm^{-1}. The UV absorption edge was found at 314 nm i.e. In the Ultra Violet region suggesting that the material has a good absorption of UV light. Also, it shows an excellent transparency in the visible region.

1. Introduction

Due to the ozone layer depletion, there is presently a strong demand for UV shielding materials which protect against the harmful effect of UV solar radiation which causes hazardous diseases to human such as skin cancer, premature aging of skin and cataract [1]. In the current era, shielding from UV irradiation by using metal oxide nanoparticles have been attracted much for its remarkable physical and chemical properties which are significantly different from their bulk counterparts [2]. Metal oxide nanoparticles such as titanium dioxide (TiO_2), zinc oxide (ZnO) and cerium oxide (CeO_2), were often studied as inorganic UV-Shilders [3]. However, the UV-blocking property of ceria nanoparticles show good shielding effect in comparison with ZnO and TiO_2 [4].

Especially, cerium oxide (CeO_2) is one of the most reactive rare earth metal oxides which possesses wide band gap energy and high refractive index in the visible region (2.1 ± 2.2) [5] which mainly made them as most prominent candidate for UV shielders. Also, Ceria changes between Ce^{3+} and Ce^{4+} states to inactivate most toxic super hydroxide radicals, hydrogen peroxide and nitroxyl radicals [6–9], and the high concentration of oxygen deficiency leads to the production of free charge carriers rapidly upon UV irradiation which decreases the photocatalytic effect [10].

Ceria nanoparticles can be synthesized by different methods such as Homogenous precipitation [11–13], Sol–gel process [14,15], Sonochemical synthesis [16,17], Thermal decomposition [18], hydrothermal synthesis [19,20], Microwave synthesis [21] and Reverse emulsion [22].

Hu et al. [23] engaged a new approach called alcohol/water mixed solution as a base for preparing nanosized ZrO_2 particles. This is due to the dielectric property of the mixed solvent which affects the nucleation and growth of Zirconia particles. Li and Gao [24] synthesized ZrO_2 (Y_2O_3) metal oxide nanoparticles by using an ethanol/water mixed solvent. The reaction rate was much higher and also the particle precipitation time was reduced as the reaction temperature increased. According to Huey-Ing Chen et.al. [25], that the particle size decreases in the following order: pure water (6.5 ± 0.9)>*t*-BuOH/water (7.4 nm)>EG/water (3.7 nm). Specifically, from the above reports it is observed that the diameter of the particles can be controlled by varying the ratio of alcohol in the reaction medium.

In this work, cerium oxide nanoparticles were synthesized by homogeneous precipitation route which has the advantages of low cost, mild synthesis conditions and easy scale-up process in which the mixer of ethylene glycol/water serves as a reaction medium. The structure, composition and particle size were characterized using XRD, Raman, SEM with EDS, TEM and AFM. Finally, the UV shielding effect of ceria nanoparticles using UV–Visible spectroscopy was examined.

* Corresponding author. Tel.: +91 4565 241538; fax: +91 4565 227713.
E-mail addresses: subramanianb3@gmail.com, bsmanian@cecri.res.in (B. Subramanian).

0925-8388/$ - see front matter © 2013 Elsevier B.V. All rights reserved.
http://dx.doi.org/10.1016/j.jallcom.2013.12.121

2. Experimental

2.1. Materials required

Chemicals used in this synthesis were Cerium (III) Nitrate hexa hydrate (purity of 99.99%,$Ce(NO_3)_2$) as a precursor, CTAB (cetyltrimethylammonium bromide) as surfactant and Monoethanolamine as a reducing agent, all chemicals being purchased from CDH chemicals and Merck TM. Ethylene glycol (>99.99% pure, Merck TM) was used as a solvent Conc. HCl was used to adjust the pH. All these chemicals were used without any further purification.

2.2. Synthesis

In a typical synthesis, 0.2 M of Cerium Nitrate and 0.2 g of CTAB were mixed in ethylene glycol (EG)/water (1:1) mixed solvent system. The reaction was performed at room temperature at a constant stirring rate. The initial pH was noted to be 7. Few drops of concentrated HCl were added to the mixture to reduce the pH to 1. Monoethanolamine was then dripped to the above solution until the pH got increased to 12. Initially a yellow solution of cerium hydroxide $Ce(OH)_3$was obtained. Slowly, this yellow color disappears and turns to purple. This is due to absorption of dissolved oxygen from air which is an intermediate mixed hydrate state. Stirring was carried out in an ambient environment for 12 h. Finally, yellow precipitate was obtained showing the complete conversion of cerium oxide nanoparticles. Then, the solution was centrifuged at 7500 rpm and washed with acetone and double distilled water for three times. It was then dried at 100 °C for 2 h in hot air oven. Further the dried powder was calcinated at 400 °C for 2 h to obtain a crystalline product.

2.3. Materials characterization

Powder XRD analysis was carried out using a Bruker AXS D8 Advance X-ray diffractometer using Cu Kα radiation (λ = 0.15406 nm) with a scintillation counter. The scanning rate was 0.05 s^{-1} in the 2θ range from 20° to 100°. The specific surface area was measured with Quantachrome Nova Win 3200e equipment by de-gassing the sample at 200 °C for 2 h and specific area was calculated by nitrogen adsorption keeping the relative pressure between 0.04 and 0.2. TEM studies were performed with a JEOL JEM-200CX instrument operating at 200 kV. EDS analysis was performed with a HITACHI S-3700N scanning electron microscope with an accelerating voltage of 20 kV. Surface morphology was examined using a XE-100 Park systems AFM, operated in a non-contact mode with a scan rate of 1 Hz. Scan size in *X* and *Y* axis was made as 1 × 1 μm. Raman spectra were collected using a Renishaw Invia Raman microscopy at room temperature. He–Ne laser beam with an excitation of 633 nm was focused under 50× objective lens and the laser spot size was about 1 μm. Raman spectra were recorded in the 200–600 cm^{-1} range with the spectral resolution of 1 cm^{-1}. The UV–Visible spectra were recorded using V-650 UV–Vis instrument from JASCO operated at room temperature in the wavelength between 200–700 nm with a scan speed of 400 nm/min.

3. Results and discussion

3.1. Structural analysis

The X-ray diffraction (XRD) pattern obtained from as-prepared and calcinated ceria is as shown in Fig. 1, the improvement in crystallinity after calcination. These peaks are in good agreement with the standard JCPDS card 43–1002 for face centered cubic structure. Before calcination as in Fig. 1b shows poor crystallinity with weak peaks viewing the presence of $Ce(OH)_4$. So the resultant sample was calcinated at 400 °C [26] where $Ce(OH)_4$ will be dehydrated directly to form CeO_2. Thus, the effect of calcination temperature shows a good crystalline growth of cerium oxide NP's with a crystalline sharp and strong diffraction peak. The diffraction peaks were all relatively broader because of the smaller size of cerium oxide nanoparticles. The crystallite size was about 9 nm calculated by using the Debye–Schrrer's formula.

From the Fig. 1c, the characteristic peaks of cerium oxide nanoparticles after calcination at 400 °C are in consistent with face centered cubic structure.

The average particle size of cerium oxide nanoparticles was examined by using TEM. The results confirmed that the particles were in spherical shape and also the size distribution was uniform with an average crystallite size of 4 nm as in Fig. 2(a). The highly crystalline nature of CeO_2 powder leads to the Debye–Scherrer diffraction rings in the Selected Area Electron Diffraction (SAED)

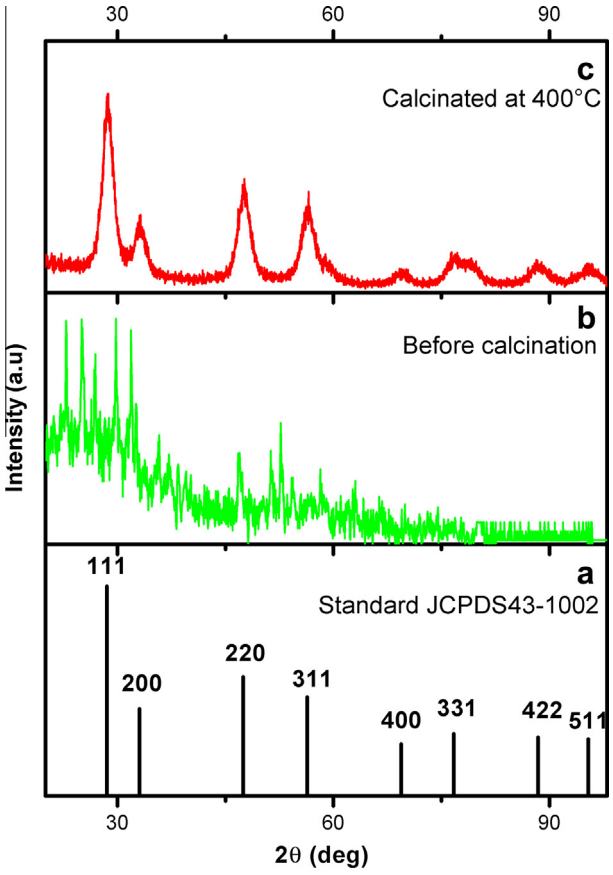

Fig. 1. XRD pattern of cerium oxide nanoparticles prepared by chemical precipitation route. (a) Reference JCPDS card 43–1002, (b) before calcination of ceria NP's, (c) after calcinated at 400 °C.

pattern as in Fig. 2(b). Like the XRD profile, the reflections were indexed to 111, 200, 220, 311, 331, 422, 611 planes respectively with a cubic CeO_2 crystal structure. In addition, all the diffraction rings match with CeO_2 powder showing absence of impurity in the system.

The specific surface area is about 139 m^2/g exhibited for cerium oxide nanoparticles measured by nitrogen adsorption with a relative pressure of 0.04–0.2. The corresponding particle size (d_{BET}) can be estimated as [11]

$$d_{BET} = 6/\rho A \quad (1)$$

where ρ is the true density of CeO_2, i.e. 7.28 g/cm^3 and *A* is the specific surface area calculated from BET. The particle size estimated from BET indicates that the average crystalline size is about 5.9 nm for CeO_2 nanoparticles.

3.2. Morphological studies

Structural morphological studies were done using SEM as shown in Fig. 3(a). It shows that nanostructured CeO_2 was nearly spherical in shape with a variety of particle sizes due to the calcination which makes the particles condense faster. Aggregates seen above are due to the accumulation of nanoparticles. It can be seen that the average diameter of the secondary particles were ~36 nm to ~50 nm respectively, along with fine particles below ~10 nm. As crystallite size was not clearly identified by using SEM further investigation was done by using TEM. The energy dispersive X-ray (EDAX) spectrum gives information about the presence of Ce and O. This confirms that the resultant sample was cerium oxide and is shown in Fig. 3(b).

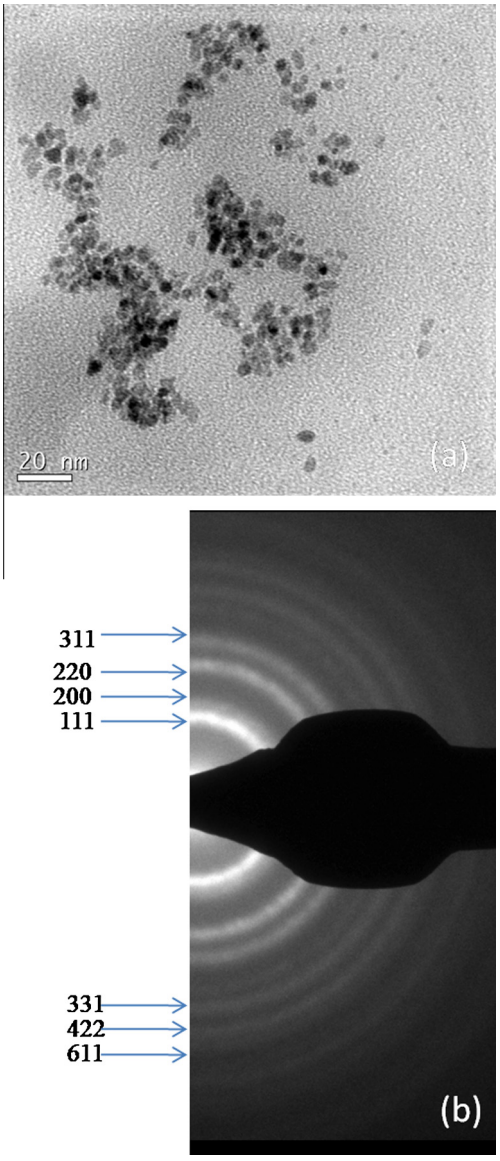

Fig. 2. (a) TEM image of cerium oxide nanoparticle calcinated at 400 °C, (b) SAED pattern.

The Surface roughness study is obtained by AFM. The obtained sample scanned in the non-contact mode of AFM across the scan size of 1 μm × 1 μm. Average Surface roughness were found to be 14.9 nm as determined by AFM. From the Fig. 4, the 3D image shows well defined particles with a granular morphology and also indicates the presence of small crystalline grains of cerium oxide nanoparticles.

3.3. Raman studies

For a comparison we did studies on resultant cerium oxide nanoparticle and commercial cerium oxide powder (size: 14 micron) from 99.99% (REO), Alfa Aesar™ (named as COP-14 sample) both shows cubic structure of $CeO_2$with a single Raman mode at 464 cm^{-1}, which is an F_2g symmetric band obtained from the space group Fm3m of a cubic fluorite structure. This is due to the symmetrical stretching mode of Ce–O8 vibrational unit [27]. From the Fig. 5, it is inferred that the increase in the asymmetry and broadening of the line features shows that the particles are of nanocrystalline size but for COP sample only narrow peak was obtained. The Raman line broadening of CeO_2 nanoparticle can be

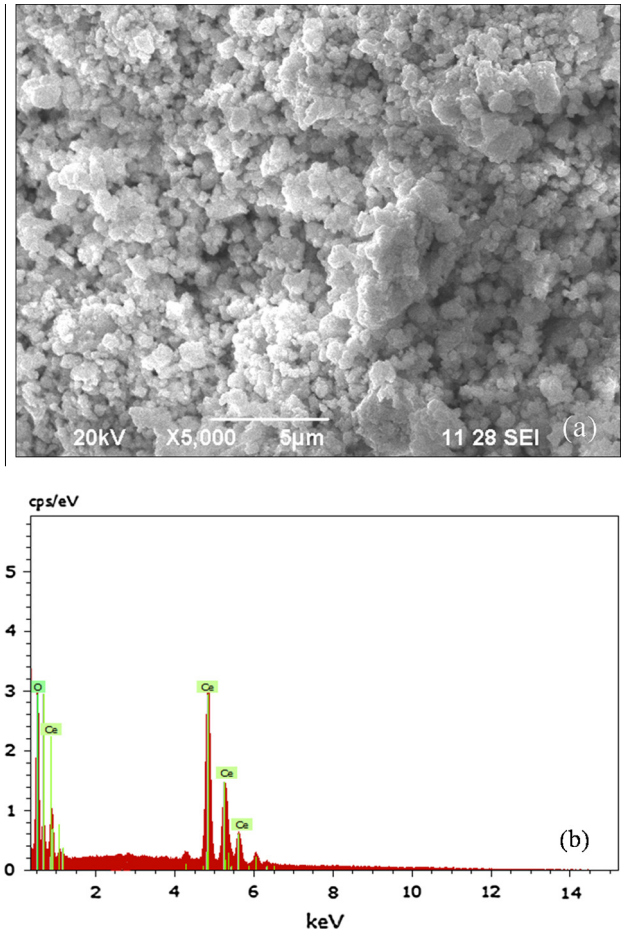

Fig. 3. (a) SEM image of the cerium oxide nanoparticles, (b) EDSspectrum.

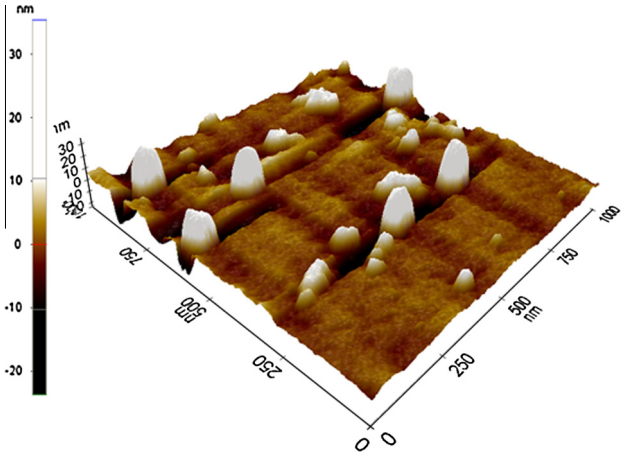

Fig. 4. AFM – three dimensional (3D) morphology of cerium oxide coated on glass substrate.

described by the dependence of the full width at half maximum, Γ, on the inverse of grain size, d_g, which follows a linear behavior [28]. Thus the obtained peaks were similar for both the samples which are in good agreement.

$$\Gamma(cm^{-1}) = 10 + \frac{124.7}{d_g} \quad (2)$$

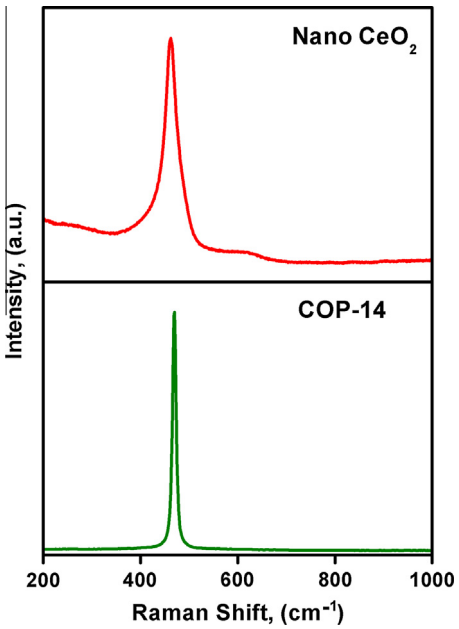

Fig. 5. Raman spectrum of cerium oxide nanoparticles and cerium oxide bulk.

Using the above relation, the grain size was calculated to be 9.5 nm which matches with the crystallite size calculated from Scherrer formula.

3.4. UV-shielding mechanism

The UV absorption mechanism of cerium oxide is based on the charge separation and recombination processes which is schematically illustrated as reported in [29] (Fig. 6). The process can be described through the following equations,

$$CeO_2 + hv \rightarrow CeO_2 \rightarrow e^- + h^+ \quad \text{(a)}$$

$$e^- + O_2 \rightarrow O_2^- \rightarrow HO_2^{\cdot} \quad \text{(b)}$$

$$h^+ + OH^- \rightarrow {\cdot}OH \quad \text{(c)}$$

where (a) Incident UV photon exits the electron from valence band to conduction band. (b) Exited electron reacts with oxygen to hydrogen ions to form superoxide. (c) Hydroxyl radicals formed by reaction of positive holes with hydroxyl ions.

The resulting cerium oxide nanoparticles (size: 4 nm) were subjected to UV–Visible measurements and for a comparison COP-14 samplewas also examined. The results show that the strong absorption has taken place in the UV region with an absorption edge located at 314 nm for cerium oxide nanoparticle and for COP-14 there is no such absorption is observed between 200–800 nm, shown in Figs. 7 and 8 compares UV transmittance spectra which points out the UV-shielding effect occurs between 200–380 nm with 0% transparency and it increases gradually from 380 nm reaching 85% up to the visible region besides no shielding effect have been observed in the UV–Visible region for COP-14 sample.

The direct band gap energy was calculated by the Estimating the value of absorption coefficient (α) to zero with

$$(\alpha E_{photon})^2 = C_{dir}(\alpha E_{photon} - E_{dir}) \quad (3)$$

where C_{dir} is the absorption constant and E_{dir} is the band gap energy for direct transition. Conventionally, the absorption coefficient (α) is defined as [18,30]

$$\alpha = \frac{2:303 Abs\rho}{Lc} = \frac{-\ln(T/100)}{t(cm)} \quad (4)$$

where *Abs* is the absorbance of the sample, *c* is the sample loading and the *L* is the path length (*L* = 1 cm). The density ρ of CeO_2, is taken as 7.28 g/cm^3, *t* = thickness.

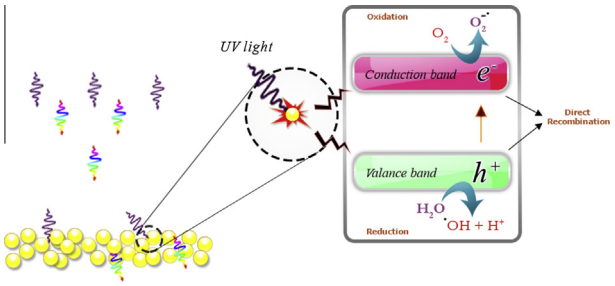

Fig. 6. Charge carrier separation (electron e^- and hole h^+) and recombination in CeO_2 by UV light irradiation (adapted from [29]).

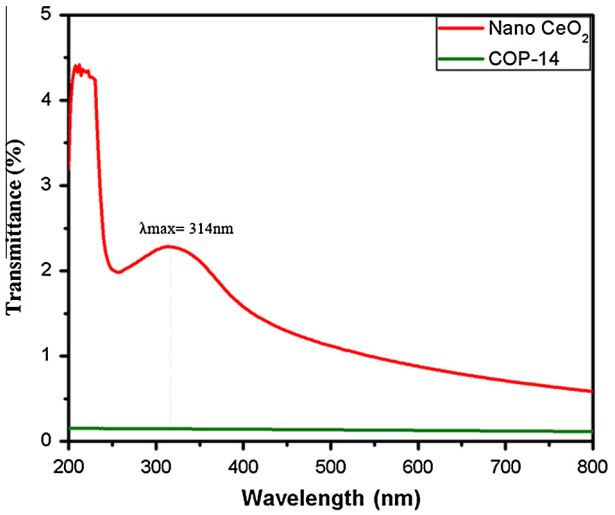

Fig. 7. UV absorption spectra of CeO_2 nanoparticles and CeO_2 bulk.

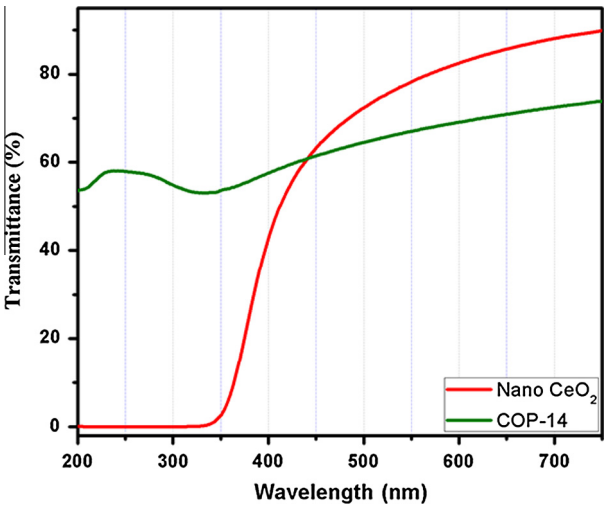

Fig. 8. Optical transmittance spectra of cerium oxide nanoparticles and CeO_2 bulk.

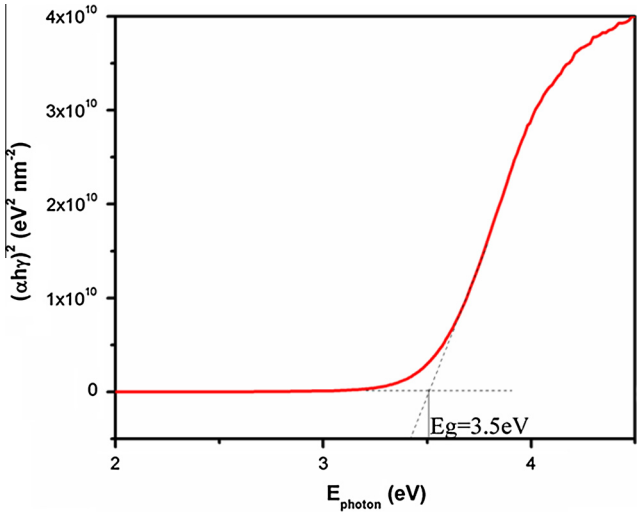

Fig. 9. Plots of $(\alpha h\gamma)^2$ versus photon energy.

From the plot of $(\alpha h\gamma)^2$ versus (E_{photon}) (Fig. 8), it reveals that the band gap was 3.5 eV. Finally from the above results it is clear that the blue shift occurred due to the quantum size effect. Thus the Nano-sized ceria particles showed both high opacity in the UV region and high transparency in the visible spectrum due to the charge transition from Oxygen and Cerium i.e. (From 2p to 4f states) in O^{2-} and Ce^{4+} (see Fig. 9) [31].

4. Conclusion

Cerium oxide nanoparticles have been successfully synthesized by the homogeneous precipitation route by employing the mixture of ethylene glycol/water as the reaction medium. The XRD pattern indicates highly crystalline structure with a cubic crystal structure. The surface area139 m^2/g was measured by using BET equipment. The EDS analysis and SEM micrograph showed the chemical compositions and surface morphology of nanoparticles. Surface morphology reveals the smooth surface with a roughness of about 14.92 nm obtained by using AFM. TEM micrograph showed accurate particle sizes with uniform size distribution of 4 nm along with spherical shaped morphology. Raman spectrum showed a strong mode at 464 cm^{-1} with F_2g symmetric band cubic structure. cerium oxide nanoparticle shows an excellent UV absorption and transparency properties in the visible region due to the increase in surface-to-volume ratio.These facts suggest that ceria nanostructures were good applicant for UV-shielders.

Acknowledgement

This work was supported by the Molecules to Materials to Devices (M2D) program, CSC 0134, funded by Council of Scientific and Industrial Research (CSIR) New Delhi.

References

[1] T. Henriksen, A. Dahlback, S.H.H. Larsen, J. Moan, Photochem. Photobiol. 51 (1990) 579–582.
[2] C. Antoniou, M.G. Kosmadaki, A.J. Stratigos, A.D. Katsambas, J. Eur. Acad. Dermatol. Venereol. 22 (2008) 1110–1118.
[3] F. Piccinno, F. Gottschalk, S. Seeger, B. Nowack, J. Nanopart. Res. 14 (2012) 1109.
[4] N.M. Zholobak, V. K Ivanov, A.B. Shcherbakov, A.S. Shaporev, O.S. Polezhaeva, A.Ye. Baranchikov, N.Ya. Spivak, Yu.D. Tretyakov, J. Photoch. Photobiol. B 102 (2011) 32.
[5] Toshiyuki Masui, Misa Yamamoto, Takao Sakata, Hirotaro Morib, Gin-ya Adachi, J. Mater. Chem. 10 (2000) 353.
[6] C. Sun, H. Li, H. Zhang, Z. Wang, L. Chen, Nanotechnology 16 (2005) 1454.
[7] C. Korsvik, S. Patil, S. Seal, W.T. Self, Chem. Commun. 14 (10) (2007) 1056.
[8] T. Pirmohamed, J.M. Dowding, S. Singh, B. Wasserman, E. Karakoti, A.S. Heckert, J.E. King, A.S. Seal, W.T. Self, Chem. Commun. 46 (16) (2010) 2736.
[9] V.K. Ivanov, A.B. Shcherbakov, I.G. Ryabokon, A.V. Usatenko, N.M. Zholobak, Yu.D. Tretyakov, Dokl. Chem. 430 (2010) 43.
[10] J.A. Rodriguez, J.C. Hanson, J.-Y. Kim, G. Liu, A. Iglesias-Juez, M.J. Fernandez-García, Phys. Chem. B 107 (2003) 3535.
[11] X.D. Zhou, W. Huebner, H.U. Anderson, Appl. Phys. Lett. 80 (20) (2002) 3814.
[12] E. Matijevi, W.P. Hsu, J. Colloid Interface Sci. 118 (2) (1987) 506.
[13] P.L. Chen, I.W. Chen, J. Am. Ceram. Soc. 76 (6) (1993) 1577.
[14] A. Verma1, N. Karar, A.K. Bakhshi, H. Chander, S.M. Shivaprasad, S.A. Agnihotry, J. Nanoparticle Res. 9 (2007) 317.
[15] X. Chu, W. Chung, L.D. Schmidt, J. Am. Ceram. Soc. 76 (1993) 2115.
[16] L. Yin, Y. Wang, G. Pang, Y. Koltypin, A. Gedanken, J. Colloid Interface Sci. 246 (2002) 78.
[17] D. Zhang, H. Fu, L. Shi, C. Pan, Q. Li, Y. Chu, W. Yu, Inorg. Chem. 46 (2007) 2446.
[18] Y. Zhou, R.J. Phillips, J.A. Switzer, J. Am. Ceram. Soc. 78 (1995) 981.
[19] Z. Yang, Y. Yang, H. Liang, L. Liu, Mater. Lett. 63 (2009) 1774.
[20] R. Yu, L. Yan, P. Zheng, J. Chen, X. Xing, J. Phys. Chem. C 112 (2008) 19896.
[21] H. Yang, C. Huang, A. Tang, X. Zhang, W. Yang, Mater. Res. Bull. 40 (2005) 1690.
[22] T. Masui, K. Fujiwara, K.I. Machida, G.Y. Adachi, T. Sakata, H. Mori, Chem. Mater. 9 (10) (1997) 2197.
[23] M.Z.C. Hu, E.A. Payzant, C.H. Byers, J. Colloid Interface Sci. 222 (2000) 20.
[24] W. Li, L. Gao, Ceram. Int. 27 (2001) 543.
[25] Huey-Ing Chen, Hung-Yi Chang, Colloids Surf A 242 (2004) 61.
[26] Jian-Chih Chena, Wen-Cheng Chenb, Yin-Chun Tiena, Chi-Jen Shihc, J. Alloys Comp. 496 (2010) 364.
[27] Li Ruixing, Shinryo Yabe, Mika Yamashita, Mater. Chem. Phys. 75 (2002) 39.
[28] J.R. McBride, K.C. Hass, B.D. Poindexter, W.H.J. Weber, Appl Phys. 76 (1994) 2435.
[29] Bertrand Faure, German Salazar-Alvarez, Anwar Ahniyaz, Irune Villaluenga, Gemma Berriozabal, Yolanda R De Miguel, Lennart Bergstom, Sci. Technol. Adv. Mater. 14 (2013) 023001.
[30] T. Hoshino, Y. Kurata, Y. Terasaki, K.J. Susa, Non-Cryst.Solids. 283 (2001) 129.
[31] Elaheh K. Goharshadi, Sara Samiee, Paul Nancarrow, J. Colloid Interface Sci. 356 (2011) 473.